

Large loss of CO₂ in winter observed across the northern
permafrost region

Susan M. Natali et al.

Deposited 2023-09-27

Citation of published version:

Natali, S. M., Watts, J. D., Rogers, B. M., Potter, S., Ludwig, S. M., Selbmann, A.-K., Sullivan, P. F., Abbott, B. W., Arndt, K. A., Birch, L., Björkman, M. P., Bloom, A. A., Celis, G., Christensen, T. R., Christiansen, C. T., Commane, R., Cooper, E. J., Crill, P., Czimczik, C., ... Zona, D. (2019). Large loss of CO₂ in winter observed across the northern permafrost region. In *Nature Climate Change* (Vol. 9, Issue 11, pp. 852–857). Springer Science and Business Media LLC.
<https://doi.org/10.1038/s41558-019-0592-8>



Published in final edited form as:

Nat Clim Chang. 2019 November ; 9: 852–857. doi:10.1038/s41558-019-0592-8.

Large loss of CO₂ in winter observed across the northern permafrost region

A full list of authors and affiliations appears at the end of the article.

Abstract

Recent warming in the Arctic, which has been amplified during the winter^{1–3}, greatly enhances microbial decomposition of soil organic matter and subsequent release of carbon dioxide (CO₂)⁴. However, the amount of CO₂ released in winter is highly uncertain and has not been well represented by ecosystem models or by empirically-based estimates^{5,6}. Here we synthesize regional *in situ* observations of CO₂ flux from arctic and boreal soils to assess current and future winter carbon losses from the northern permafrost domain. We estimate a contemporary loss of 1662 Tg C yr⁻¹ from the permafrost region during the winter season (October through April). This loss is greater than the average growing season carbon uptake for this region estimated from process models (–1032 Tg C yr⁻¹). Extending model predictions to warmer conditions in 2100 indicates that winter CO₂ emissions will increase 17% under a moderate mitigation scenario—Representative Concentration Pathway (RCP) 4.5—and 41% under business-as-usual emissions scenario—RCP 8.5. Our results provide a new baseline for winter CO₂ emissions from northern terrestrial regions and indicate that enhanced soil CO₂ loss due to winter warming may offset growing season carbon uptake under future climatic conditions.

Air and soil temperatures in the Arctic are increasing rapidly, with the most severe climate amplification occurring in autumn and winter^{1,2}. Although warmer soils decompose more quickly, thus releasing more CO₂ into the atmosphere, microbial respiration is known to occur even under extremely cold winter conditions (e.g., down to ~ –20°C) in unfrozen microsites that can persist at sub-zero soil temperatures⁷. This production and release of CO₂ in winter is expected to increase substantially as soils continue to warm and thaw under a warming climate^{4,8}.

Users may view, print, copy, and download text and data-mine the content in such documents, for the purposes of academic research, subject always to the full Conditions of use:http://www.nature.com/authors/editorial_policies/license.html#terms

*Correspondence to: snatali@whrc.org.

†Authors contributed equally to this work.

Author contributions: S.M.N., J.D.W., and B.M.R. conceived the work. B.W.A., G.C., C.T.C., H.G., E.E.J., M.M.L., S.M.L., M.L., A.M., C.M., S.M.N., F.R., B.M.R., K.S., A.S., C.C.T., Y.W., and X.X. extracted unpublished data. K.A.A., M.P.B., G.C., T.R.C., E.J.C., C.T.C., S.D., J.D., J.E.E., B.E., E.S.E., T.F., M.G., J.P.G., P.G., M.H., J.D.J., A.A.A.K., Y.K., L.K., K.S.L., M.L., R.M., J.M., A.M., S.M.N., W.C.O., F.W.P., N.P., W.Q., D.R., T.S., N.M.S., E.A.G.S., P.R.S., O.S., P.F.S., M.P.W., C.W., and D.Z. provided unpublished or raw data. L.B., A.A.B., J.D., J.S.K., Z.L., N.M., A.D.M., B.P., and Z.Z. provided modeled data/results. S.M.L., C.M., S.M.N., S.P., and J.D.W. prepared tables and figures. G.C., H.G., M.J.L., M.M.L., S.M.L., S.M.N., S.P., B.M.R., P.F.S., and J.D.W. performed statistical analyses, including BRT modeling. S.P., B.M.R., and J.W. led the BRT upscaling or projection analyses. All authors contributed to data interpretation and preparation of manuscript text.

Data Availability: Data are archived and freely available at the ORNL Distributed Active Archive Center (DAAC). The synthesis dataset is available at <https://doi.org/10.3334/ORNLDAAC/1692>. Monthly carbon flux maps (25 km, October–April, 2003–2018; 2018–2100 for RCP 4.5 and RCP 8.5) are available at <https://doi.org/10.3334/ORNLDAAC/1683>.

However, it remains highly uncertain how much CO₂ is currently emitted from the permafrost region during winter⁹ and how much these emissions might increase in the future^{8,10}. Many ecosystem models are not well adapted to simulate respiration from high latitude soils⁵ and may greatly underestimate present and future winter CO₂ emissions⁶. Given the limitations in current models, lack of satellite and airborne CO₂ data for the Arctic during winter¹¹, and gaps in spatial coverage of Arctic air monitoring networks¹², *in situ* CO₂ flux observations provide the most direct insight into the state of winter CO₂ emissions across the northern permafrost domain.

Studies of winter respiration indicate that the amount of CO₂ released during cold periods depends greatly on vegetation type¹³, availability of labile carbon substrates^{14,15,16}, non-frozen soil moisture^{4,7,15,17,18}, microbial community composition and function¹⁹, and snow depth^{15, 20, 21}. However, knowledge of the influence of these drivers on the rates and patterns of winter CO₂ flux on a regional scale remains limited^{6, 9}.

Here we present a new compilation of *in situ* CO₂ winter flux data for the northern permafrost domain (Fig. 1, Supplementary Information (SI) Table 1) to examine the drivers and magnitude of winter respiration in the Arctic. We define the winter period as October through April—months when the landscape is generally covered by snow and photosynthesis is negligible^{22,23}. The dataset represents more than 100 high latitude sites and comprises more than 1,000 aggregated monthly fluxes. We examined patterns and processes driving winter CO₂ emissions and scaled fluxes to the permafrost domain using a boosted regression tree (BRT) machine learning model based on hypothesized drivers of winter CO₂ flux. Environmental and ecological drivers (e.g., vegetation type and productivity, soil moisture, and soil temperature) obtained from satellite remote sensing and reanalysis data were used to estimate regional winter CO₂ emissions for contemporary (2003–2017) climatic conditions. We estimated winter fluxes through 2100 using meteorological and carbon cycle drivers from ensembles of Earth System Model (ESM) outputs for RCP 4.5 and RCP 8.5²⁴.

Soil temperature had the strongest influence on winter CO₂ emissions, with fluxes measured at soil temperatures down to –20°C (Fig. 2a), in line with results from lab incubations (Fig. 2b), demonstrating that microbial respiration may occur in unfrozen microsites that persist at sub-zero bulk soil temperatures¹⁸. Diffusion of stored CO₂ produced during the non-frozen season may have driven some of the emissions measured in winter, but the magnitude of this contribution is unclear. Winter CO₂ emissions increased by a factor of 2.9 (95% credible interval (CI) = 2.1, 4.2) per 10°C soil temperature increase (i.e., Q10) for *in situ* fluxes and by a factor of 8.5 (CI= 5.0, 14.5) for CO₂ release from low temperature lab incubations. Differences between *in situ* and lab Q10s may reflect site-level differences in environmental drivers other than temperature (*in situ* and lab sites were not fully overlapping), experimental design differences (e.g., less restricted diffusion in the lab), or variation in the depth of *in situ* CO₂ production, which can occur throughout the soil profile, relative to the depth of recorded temperature, which tended to be closer to the soil surface (~ 10 cm).

Air and soil temperatures had the strongest influence on winter flux with a combined relative influence (RI) of 32%. Vegetation type (15% RI), leaf area index (LAI; 11%), tree cover

(TC; 10%), and previous summer's gross primary productivity (GPP; 8.5%) also influenced winter CO₂ emissions (SI Fig. 1). Along with warmer air and soil temperatures in winter and corresponding increases in CO₂ loss, summer GPP has also been increasing in some parts of the northern permafrost region²⁵. The positive relationship between GPP and winter CO₂ emissions suggests that increased CO₂ uptake during the growing season may be offset, in part, by winter CO₂ emissions.

Another important driver of winter respiration was unfrozen water content, which is a function of soil temperature and texture, as finer textured soils contain more unfrozen water than coarse soils for a given sub-zero temperature²⁶. Indirect measurements of unfrozen water availability confirm its importance: soils with low sand and high clay content, which tend to have greater unfrozen microsites, were characterized by higher CO₂ flux rates. While snow cover is a key driver of winter flux through its impact on ground temperature²⁷, remote sensing estimates of snow cover were not significant predictors in the model; this may be a result of high uncertainty in regional snow products or because snow depth and density, which are difficult to determine from space using currently available satellite technology²⁸, have a greater influence on ground temperatures than snow presence alone.

Using our model to assess winter flux for the terrestrial permafrost domain, we estimate approximately 1662 Tg C winter⁻¹ released under current climatic conditions (2003–2017), with a corresponding uncertainty of 813 Tg C winter⁻¹ (SI Methods). We observed no temporal trends in winter CO₂ flux during this 15-year period ($p > 0.1$), which corresponded with the lack of a significant circumpolar trend in the reanalysis winter air or soil temperature data used as model inputs ($p > 0.1$). Although we did not observe region-wide trends during the past 15 years, atmospheric CO₂ enhancements for Alaska⁸ and site-level studies from Alaskan tundra^{29,30} showed recent increases in winter emissions, which are already shifting some tundra regions from an annual carbon sink to a source.

Our flux estimates are twofold higher than a previous estimate derived from *in situ* measurements reported in the Regional Carbon Cycle Assessment and Processes (RECCAP) tundra and northern boreal domain¹⁰, which was based on a much smaller dataset (< 20 site-years for winter data). The RECCAP study reported fluxes of 24 – 41 g C m⁻² winter⁻¹ from *in situ* data, compared to 64 g C m⁻² winter⁻¹ estimated here for the RECCAP region and 98 g C m⁻² winter⁻¹ for the full permafrost domain (SI Fig. 2). Our estimate of winter flux agrees more closely with the RECCAP atmospheric inversion estimate (27–81 g C m⁻² winter⁻¹), providing some closure between bottom-up and top-down assessments^{6,12}.

We then compared our permafrost region flux estimates to winter net ecosystem exchange (NEE) outputs from five process-based terrestrial models and from FluxCom, a global machine-learning NEE product³¹. Our winter CO₂ flux estimate was generally higher than estimates from these models, which ranged from 377 Tg C winter⁻¹ for FluxCom and from 503 to 1301 Tg C for the process models (mean: 1008 Tg C winter⁻¹; SI Fig. 3). Similar variation in carbon budget estimates from terrestrial models has been reported elsewhere for high latitude regions⁵, which reflects considerable differences in model parameterization of soil temperature, unfrozen water, and substrate effects on CO₂ production under winter conditions. Some process-based models may underestimate winter CO₂ emissions by

shutting down respiration at sub-zero soil temperatures³² or because they are unable to capture small-scale processes that influence winter flux, such as talik formation and shrub-snow interactions that are more likely to be captured by *in situ* measurements.

Combining growing season NEE (-687 to -1647 Tg C season⁻¹) and winter NEE derived from the process-based terrestrial models described above results in an estimated annual NEE of -351 to 514 Tg C yr⁻¹ (-555 for FluxCom; SI Table 2). Because our winter emissions estimate was higher than these process models, we expect that annual CO₂ losses may also be higher. For example, if we account for growing season NEE using the process model estimates, this would yield an average annual CO₂ emission of 646 Tg C yr⁻¹ (range of 15 to 975) from the permafrost region, based on our estimate of winter CO₂ flux.

Our assessment of future winter emissions—obtained by forcing the BRT model with environmental conditions from CMIP5 ESM outputs²—showed significant increases in winter CO₂ emissions under both climate scenarios ($p < 0.001$, Fig. 3); however, emissions were substantially lower with climate mitigation in RCP 4.5 than with RCP 8.5. Compared to current winter emissions (2003–2017), there was a 17% projected increase in winter CO₂ flux under RCP 4.5 by 2100 (to 1950 Tg C yr⁻¹) and a 41% increase under RCP 8.5 by 2100 (to 2345 Tg C yr⁻¹) (Fig. 4).

The present-day continuous permafrost zone experienced the strongest positive trend in winter CO₂ emissions under both climate scenarios ($p < 0.001$); however, accounting for differences in area, the largest rate of change in winter CO₂ emissions occurred across the discontinuous zone (SI Table 3) where soils have warmed rapidly and permafrost has diminished in recent years³³. The differences in projected changes in winter CO₂ emissions among permafrost zones may reflect the influence of latitudinal variation in environmental and ecological variables, including tree cover, dominant vegetation, and soil organic matter content and composition³⁴.

Increased winter CO₂ emissions from our data-driven BRT model were largely driven by changes in soil and air temperatures, which both increased by $0.04^{\circ}\text{C yr}^{-1}$ under RCP 4.5, and increased by $0.08^{\circ}\text{C yr}^{-1}$ for soil and $0.1^{\circ}\text{C yr}^{-1}$ for air under RCP 8.5 (SI Fig. 4). Vegetation leaf area and GPP, both of which were positively related to winter CO₂ flux, also significantly increased through 2100.

From 2018 to 2100, we estimated a cumulative winter flux of 150 Pg C for RCP 4.5 and 162 Pg C for RCP 8.5. This represents an additional 15 Pg C for RCP 4.5 and 27 Pg C for RCP 8.5 emitted as a result of climate change, when compared to the estimated 135 Pg of C that would be emitted through 2100 if current (2003–2017) climatic conditions remained constant. These losses are comparable to 70% of the current permafrost-region near-surface (0–30cm) soil carbon pool³⁵. These projected increases are substantially lower than projections from CMIP5 ESMs, in which winter CO₂ emissions from ecosystem respiration for the permafrost region (1753 ± 1066 Pg C yr⁻¹ for 2003–2005) were projected to increase in 2100 by 37% and 86% under RCP 4.5 (2482 ± 1403 Pg C yr⁻¹) and 8.5 (3473 ± 1731 Pg C yr⁻¹), respectively (Fig. 4). Our data-driven BRT model may provide more conservative estimates because current *in situ* observations may not adequately reflect

future environmental responses to substantially warmer winter conditions. However, it is also possible that the ESMs are missing stabilizing drivers and mechanisms that might provide negative feedbacks to winter CO₂ emissions. Hence, we stress the importance of addressing current uncertainties in process-model estimates of both growing season and winter CO₂ exchange. Given the data limitations during the winter, there is a particular need for long-term monitoring of winter CO₂ exchange in permafrost regions to provide key insights into processes that may enhance or mitigate change. As most of the CMIP5 models do not currently include a permafrost component, these data are critical for improving pan-arctic carbon cycle simulations.

Some of the projected winter CO₂ emissions could be offset by plant carbon uptake, which is expected to increase as plants respond favorably to warming and CO₂ fertilization^{36,37}. In addition, our modeled results do not explicitly account for CO₂ uptake during the shoulder seasons (early and late winter period, e.g., October and April), which can occur, even under the snowpack^{22,23,38} and which may increase with climate warming²². Our model projections also did not incorporate all changes expected under future climates, such as changes in permafrost distribution, delayed seasonal freeze-up, increased fire frequency, changes in snow cover and distribution, thermokarst frequency and extent, and landscape-level hydrologic changes (e.g., lake drainage).

The CO₂ emissions reported here are only part of the winter carbon budget, which also includes significant CH₄ emissions from land^{17,39} and CO₂ and CH₄ emissions from inland waters⁴⁰. Recent data-derived estimates of high-latitude terrestrial winter CH₄ emissions range from 1.6 Tg C yr⁻¹ (land area > 60°N)³⁹ to 9 Tg C yr⁻¹ for arctic tundra¹⁷. Similar to winter CO₂ emissions, process models significantly underestimated the fraction of annual CH₄ emissions released during the winter³⁹.

To reduce uncertainty in estimates of current and future emissions, we recommend increased spatial and temporal coverage, and coordination and standardization of *in situ* winter measurements, improvements to regional snow density products, and development of remote sensing active sensors that can detect high resolution (< 20 km) changes in atmospheric CO₂ concentrations during periods of low to no sunlight, which is a key constraint on efforts to monitor changes in permafrost region carbon cycling. Current rates of winter CO₂ emissions may be offsetting CO₂ uptake by vegetation across the permafrost region. Circumpolar winter CO₂ emissions will likely increase in the near future as temperatures continue to rise; however, this positive feedback on global climate can be mitigated with a reduction of global anthropogenic greenhouse gas emissions.

Methods

Data overview

We compiled a dataset of *in situ* winter season (Oct-April) CO₂ emissions and potential driving variables from sites within the northern permafrost zone⁴¹. The synthesized dataset included 66 published studies and 21 unpublished studies (SI Table 1) conducted at 104 sites (*i.e.*, sample areas with unique geographic coordinates) and in 152 sampling locations (*i.e.*, different locations within a site as distinguished by vegetation type, landscape position,

etc.) Sites spanned boreal and tundra landcover classes (SI Fig. 5, SI Table 4) in continuous permafrost (n=69), discontinuous (n=24), and isolated/sporadic (n=11) permafrost zones (Fig. 1). Data were aggregated at the monthly level; however, the number of measurements per month varied among studies. The dataset included more than 1,000 site-month flux measurements. We also extracted CO₂ data from incubations of permafrost-region soils (SI Table 5) to compare their temperature response functions (Q10) with Q10 derived from the synthesized *in situ* flux data. Further details of data extraction and Q10 calculations can be found in the Supplementary Methods.

Data extraction, geospatial data

We extracted data from regional gridded geospatial products including climatological data, soil temperature and moisture, snow water equivalent, soil carbon stocks and texture, permafrost status, vegetation cover, proxies of vegetation growth and productivity (*e.g.*, enhanced vegetation index, EVI; leaf area index, LAI; gross primary productivity, GPP). See Supplementary Methods for further description and data sources. All geospatial data were re-gridded to the National Snow and Ice Data Center Equal Area Scalable Earth (EASE) 2.0 format⁴² at a 25-km spatial resolution prior to the CO₂ flux upscaling and simulations.

Boosted regression tree analysis

We used boosted regression tree analysis (BRT) to model drivers of winter CO₂ emissions and to upscale emissions to the northern permafrost region under current and future climate scenarios. The BRT model was fit in R⁴³ using ‘gbm’ package version 2.1.1⁴⁴, and using code adapted from⁴⁵. The BRT model was fitted with the following metaparameters: Gaussian error distribution, bag-fraction (*i.e.*, proportion of data used in each iteration) of 0.5, learning rate (contribution of each tree to the final model) of 0.005, and a tree complexity (maximum level of interactions) of two. We used 10-fold cross-validation (CV) to determine the optimal number of trees to achieve minimum predictive error and to fit the final model to the data.

We used geospatial data as explanatory variables in our BRT model (See Supplementary Methods for full description of input data). We removed highly correlated variables from the models (Spearman $\rho = 0.7$), retaining the variable within each functional category (*e.g.*, air temperature) that had the highest correlation with winter flux. We further reduced the model by removing variables in reverse order of their relative influence, until further removal resulted in a 2% average increase in predictive deviance. We compared this model with one in which we included site level *in situ* data as explanatory variables. We used the geospatial model because it allowed us to upscale results and because the percent deviance (SI Table 6) and driving variables (SI Fig. 1) were similar between models.

We assessed BRT model performance using: 1. The correlation between predicted and observed values using the CV data (*i.e.*, data withheld from model fitting), hereafter referred to as the CV correlation, and; 2. deviance explained by the model over the evaluation dataset (*i.e.*, CV data), calculated as: % deviance = (CV null deviance - CV residual deviance)/CV null deviance * 100. Further details of the BRT models can be found in the Supplementary Methods.

We obtained an estimate of model uncertainty by first obtaining the average internal root mean squared error (RMSE; $0.21 \text{ g C m}^{-2} \text{ d}^{-1}$) for the ensemble of boosted regression trees. We then made the assumption that this error applied equally to all grid cell areas within the domain. Scaling this error to the full domain ($16.95 \times 10^6 \text{ km}^2$) and by the total number of days for the winter (October through April) period provided us with a winter flux error of $813 \text{ Tg C winter}^{-1}$.

Spatial and temporal domain for mapping

We scaled the modeled flux data to the northern permafrost land area 49° N^{41} , which comprises $16.95 \times 10^6 \text{ km}^2$ of tundra and boreal lands (excludes glaciers, ice sheets, and barren lands; Fig. 1) with lake area removed. We defined the winter period as the months of October through April. Because the climate within this timeframe varies substantially across the permafrost zone, this month-based definition, while temporally consistent, may include some areas that are influenced by climate that would fall outside expected winter temperature ranges. Therefore, in a separate approach (presented in the Supplementary Method), we defined winter based on soil temperature, but we did not find substantial differences in regional flux budgets when using the two approaches (temperature-defined winter flux was $\sim 5\%$ higher, $1,743 \text{ Tg C}$, than when using the month-based winter period).

Spatial upscaling of fluxes

The BRT model was applied at a monthly time step from 2003 through 2017. For each month, the map predictions were applied to a raster stack of input predictors using the R ‘dismo’ package⁴⁶ for interface with the ‘gbm’ package and the ‘raster’ v2.6–7 predict function for geospatial model applications. A n.tree (# of trees) of 1,000 was selected for each model run. Output monthly mean estimates of daily CO_2 flux ($\text{g CO}_2\text{-C m}^{-2} \text{ d}^{-1}$) were generated for each 25-km grid cell. Total pan-arctic CO_2 flux was obtained on a monthly basis by first calculating the terrestrial area for each grid cell by subtracting lake fractions (MODIS satellite product MOD44W) from each grid cell area. The fluxes were then scaled according to days per month and terrestrial area to obtain per grid cell totals.

We analyzed the pan-arctic flux data for annual temporal trends using the nonparametric Mann-Kendall test, which was run in the R ‘zyp’ package⁴⁷ with pre-whitening (Yue and Pilon method) to remove autocorrelation. We report Kendall’s correlation coefficient, τ , to describe the strength of the time-series and Theil-Sen slope to describe trends over time.

Comparison of BRT estimates with process-based models

We compared our regional winter flux estimates to: 1) outputs from five process-based terrestrial models estimated for the northern permafrost domain: National Center for Atmospheric Research (NCAR) Community Land Model (CLM) versions 4.5 and 5; Lund-Potsdam-Jena Dynamic Global Vegetation Model (LPJ-DGVM), Wald Schnee und Landschaft version (LPJ-wsl); CARbon DATA MOdel FraMework (CARDAMOM); and the NASA SMAP Level 4 Carbon (L4C) Version 3 product; 2) estimates for the northern permafrost domain derived from FluxCom, a global gridded machine-learning net ecosystem exchange (NEE) product; and 3) four process-based terrestrial models and eight atmospheric inversion models from the high latitude model intercomparison for the Regional Carbon

Cycle Assessment and Processes (RECCAP) tundra and northern boreal domain¹⁰. See Supplementary Methods for further description of these models.

Projected CO₂ flux

Inputs for the BRT model of future scenarios of winter CO₂ flux were obtained from ensembles of Earth System Model (ESM) outputs from the Fifth Coupled Model Intercomparison Project (CMIP5) for RCP 4.5 and 8.5². Inputs included: 1) Annual GPP; 2) mean annual summer LAI (July & August); 3) mean summer soil moisture (June, July, August); 4) mean monthly soil moisture; 5) mean monthly near-surface (2 m) air temperature; and 6) mean monthly soil temperature (layer 1) (SI Table 7). Ensemble mean RCP 4.5 and 8.5 predictor fields were bias-corrected using the delta, or perturbation method⁴⁸, based on historic ESM outputs and observed historical data and re-projected to EASE2 25 km grids.

In addition to the 0.21 g C m⁻² d⁻¹ error obtained based on the BRT model RMSE, we used the outcome from bootstrapped BRT model simulations to estimate additional, inherit prediction variability in the machine learning outcomes for current and future CO₂ emissions⁴⁹ (see Supplementary Information).

For the CMIP5 RCP 4.5 and 8.5 simulations of respiration, we used an r1i1p1 ensemble mean from 15 models (see Supplementary Information).

Supplementary Material

Refer to Web version on PubMed Central for supplementary material.

Authors

Susan. M. Natali^{1,*†}, Jennifer D. Watts^{1,†}, Brendan M. Rogers¹, Stefano Potter¹, Sarah M. Ludwig¹, Anne-Katrin Selbmann², Patrick F. Sullivan³, Benjamin W. Abbott⁴, Kyle A. Arndt⁵, Leah Birch¹, Mats P. Björkman⁶, A. Anthony Bloom⁷, Gerardo Celis⁸, Torben R. Christensen⁹, Casper T. Christiansen¹⁰, Roisin Commane¹¹, Elisabeth J. Cooper¹², Patrick Crill¹³, Claudia Czimczik¹⁴, Sergey Davydov¹⁵, Jinyang Du¹⁶, Jocelyn E. Egan¹⁷, Bo Elberling¹⁸, Eugenie S. Euskirchen¹⁹, Thomas Friborg²⁰, H el ene Genet¹⁹, Mathias G ockede²¹, Jordan P. Goodrich^{5,22}, Paul Grogan²³, Manuel Helbig^{24,50}, Elchin E. Jafarov²⁵, Julie D. Jastrow²⁶, Aram A. M. Kalhori⁵, Yongwon Kim²⁷, John Kimball¹⁶, Lars Kutzbach²⁸, Mark J. Lara²⁹, Klaus S. Larsen²⁰, Bang-Yong Lee³⁰, Zhihua Liu³¹, Michael M. Lorant³², Magnus Lund⁹, Massimo Lupascu³³, Nima Madani⁷, Avni Malhotra³⁴, Roser Matamala²⁶, Jack McFarland³⁵, A. David McGuire¹⁹, Anders Michelsen³⁶, Christina Minions¹, Walter C. Oechel^{5,37}, David Olefeldt³⁸, Frans-Jan W. Parmentier^{39,40}, Norbert Pirk^{39,40}, Ben Poulter⁴¹, William Quinton⁴², Fereidoun Rezanezhad⁴³, David Risk⁴⁴, Torsten Sachs⁴⁵, Kevin Schaefer⁴⁶, Niels M. Schmidt⁴⁷, Edward A.G. Schuur⁸, Philipp R. Semenchuk⁴⁸, Gaius Shaver⁴⁹, Oliver Sonntag⁵⁰, Gregory Starr⁵¹, Claire C. Treat⁵², Mark P. Waldrop³⁵, Yihui

Wang⁵, Jeffrey Welker^{53,54}, Christian Wille⁴⁵, Xiaofeng Xu⁵, Zhen Zhang⁵⁵, Qianlai Zhuang⁵⁶, Donatella Zona^{5,57}

Affiliations

¹Woods Hole Research Center, Falmouth, MA 02540, USA.

²University of Bayreuth, Bayreuth, Germany.

³Environment and Natural Resources Institute, University of Alaska, Anchorage, AK 99508, USA.

⁴Brigham Young University, Department of Plant and Wildlife Sciences, Provo, UT 84602, USA.

⁵Department of Biology, San Diego State University, San Diego, CA 92182, USA.

⁶Department of Earth Sciences, University of Gothenburg, PO Box 460, SE-405 30 Göteborg, Sweden.

⁷Jet Propulsion Laboratory, California Institute of Technology, Pasadena, CA 91109, USA.

⁸Center for Ecosystem Science and Society, Northern Arizona University, Flagstaff, AZ 86001, USA.

⁹Department of Bioscience, Arctic Research Centre, Aarhus University, Frederiksborgvej 399, 4000 Roskilde, Denmark.

¹⁰NORCE Norwegian Research Centre, Bjerknes Centre for Climate Research, Bergen, Norway.

¹¹Dept. of Earth & Environmental Sciences of Lamont-Doherty Earth Observatory at Columbia University, Palisades, NY 10964, USA.

¹²Department of Arctic and Marine Biology, Faculty of Biosciences, Fisheries and Economics, UiT. The Arctic University of Norway, N9037 Tromsø, Norway.

¹³Dept. of Geological Sciences and Bolin Centre for Climate Research, Stockholm University, Sweden.

¹⁴Earth System Science, University of California, Irvine, CA 92697, USA.

¹⁵Northeast Science Station, Pacific Geographical Institute, Cherskii, Russia.

¹⁶Numerical Terradynamic Simulation Group, W.A. Franke College of Forestry & Conservation, University of Montana, Missoula, MT 59812, USA.

¹⁷Department of Earth Sciences, Dalhousie University, Halifax, NS, Canada.

¹⁸Center for Permafrost (CENPERM), Department of Geosciences and Natural Resource Management, University of Copenhagen, Øster Voldgade 10, DK-1350 Copenhagen, Denmark.

¹⁹University of Alaska Fairbanks, Institute of Arctic Biology, Fairbanks, AK 99775, USA.

- ²⁰Department of Geosciences and Natural Resource Management, University of Copenhagen, Denmark.
- ²¹Max Planck Institute for Biogeochemistry, Jena, Germany.
- ²²Scripps Institution of Oceanography, UCSD, La Jolla, CA 92037, USA.
- ²³Department of Biology, Queen's University, Kingston, ON, Canada.
- ²⁴McMaster University, School of Geography and Earth Sciences, Hamilton, ON, L8S 4K1.
- ²⁵Earth and Environmental Sciences Division, Los Alamos National Laboratory, Los Alamos, New Mexico 87545, USA.
- ²⁶Environmental Science Division, Argonne National Laboratory, Argonne, IL 60439, USA.
- ²⁷International Arctic Research Center, University of Alaska Fairbanks, AK 99775, USA.
- ²⁸Institute of Soil Science, Universität Hamburg, Hamburg, Germany.
- ²⁹Department of Plant Biology, University of Illinois, Urbana, IL 61801, USA.
- ³⁰Korea Polar Research Institute (KOPRI), Incheon 21990, Republic of Korea)
- ³¹CAS Key Laboratory of Forest Ecology and Management, Institute of Applied Ecology, Chinese Academy of Sciences, Shenyang, 110016, China
- ³²Department of Geography, Colgate University, Hamilton, NY 13346, USA.
- ³³Department of Geography, National University of Singapore, Singapore 117570.
- ³⁴Department of Earth System Science, Stanford University, Stanford, CA 94305.
- ³⁵Geology, Minerals, Energy, and Geophysics Science Center, U.S. Geological Survey, Menlo Park, CA 94025, USA.
- ³⁶Department of Biology, University of Copenhagen, Denmark.
- ³⁷University of Exeter, Exeter, UK.
- ³⁸University of Alberta, Department of Renewable Resources, Edmonton, Alberta, Canada.
- ³⁹Department of Geosciences, University of Oslo, Oslo, Norway.
- ⁴⁰Department of Physical Geography and Ecosystem Science, Lund University, Lund, Sweden.
- ⁴¹NASA GSFC, Biospheric Sciences Lab., Greenbelt, MD 20771, USA.
- ⁴²Wilfrid Laurier University, Waterloo, Ontario, Canada.
- ⁴³Ecology Research Group, Water Institute and Department of Earth & Environmental Sciences, University of Waterloo, 200 University Avenue West, Waterloo, ON, N2L 3G1, Canada.

- ⁴⁴St. Francis Xavier University, Antigonish, Nova Scotia, Canada.
- ⁴⁵GFZ German Research Centre for Geosciences, Telegrafenberg, Potsdam, Germany.
- ⁴⁶National Snow and Ice Data Center, Boulder, CO 80309, USA.
- ⁴⁷Arctic Research Centre, Department of Bioscience, Aarhus University, Roskilde, Denmark.
- ⁴⁸Division of Conservation Biology, Vegetation Ecology and Landscape Ecology, Department of Botany and Biodiversity Research, Rennweg 14, 1030 Vienna, Austria.
- ⁴⁹The Ecosystems Center, Marine Biological Laboratory, Woods Hole, MA 02543, USA.
- ⁵⁰Université de Montréal, Département de géographie & Centre d'études nordiques, 520 chemin de la Côte Sainte Catherine, Montréal, QC H2V 2B8.
- ⁵¹Department of Biological Sciences, University of Alabama, Tuscaloosa, AL 35487, USA.
- ⁵²Department of Environmental and Biological Science, University of Eastern Finland, Finland.
- ⁵³Department of Biological Sciences, University of Alaska Anchorage, Anchorage, AK 99508, USA.
- ⁵⁴Ecology and Genetics Research Unit, University of Oulu, Finland and UArctic.
- ⁵⁵Department of Geographical Sciences, University of Maryland, College Park, MD 20742, USA.
- ⁵⁶Department of Earth, Atmospheric and Planetary Sciences, Purdue University, West Lafayette, IN 47907, USA.
- ⁵⁷University of Sheffield, Sheffield, UK.

Acknowledgements:

This study was supported by funding from NASA's Arctic-Boreal Vulnerability Experiment (ABOVE; #NNX15AT81A to S.M.N.), with additional funding from NASA NIP (NNX17AF16G TO J.D.W.), NSF (#955713 and #1331083 to E.A.G.S.; # 1503559 to E.E.J.), the Next-Generation Ecosystem Experiments Arctic project, DOE Office of Science (E.E.J.), NRF of Korea (NRF-2016M1A5A1901769; KOPRI-PN-19081; B.Y.L., Y.K.), and funding that supported the data that were included in this synthesis.

References

1. Huang J. Recently amplified arctic warming has contributed to a continual global warming trend. *Nat. Clim. Change* 7, 875–879 (2017).
2. Koenigk T. et al. Arctic climate change in 21st century CMIP5 simulations with EC-Earth. *Clim. Dyn* 40, 2719–2743 (2013).
3. Cohen J, Screen JA, Furtado JC, Barlow M, et al. Recent Arctic amplification and extreme mid-latitude weather. *Nature Geosci.* 7, 627–637 (2014).

4. Schadel C, Bader MK-F, Schuur EAG, Biasi C, Bracho R. et al. Potential carbon emissions dominated by carbon dioxide from thawed permafrost soils. *Nat. Clim. Change* 6, 950–953 (2016).
5. Fisher JB et al. Carbon cycle uncertainty in the Alaskan Arctic. *Biogeosciences* 11, 4271–4288 (2014).
6. Commane R, Lindaas J, Benmergui J, Luus KA, et al. Carbon dioxide sources from Alaska driven by increasing early winter respiration from Arctic tundra. *Proc. Natl. Acad. Sci* 114, 5361–5366 (2017). [PubMed: 28484001]
7. Elberling B, Brandt KK Uncoupling of microbial CO₂ production and release in frozen soil and its implications for field studies of arctic C cycling. *Soil Biol. Biogeochem* 35, 263–272 (2003).
8. Schuur EAG, McGuire AD, Schadel C, Grosse G, et al. Climate change and the permafrost carbon feedback. *Nature* 520, 171–179 (2015). [PubMed: 25855454]
9. Belshe EF, Schuur EAG, Bolker BM Tundra ecosystems observed to be CO₂ sources due to differential amplification of the carbon cycle. *Ecology Lett.* 16, 1307–1315 (2013).
10. McGuire AD et al. An assessment of the carbon balance of Arctic tundra: Comparisons among observations, process models, and atmospheric inversions. *Biogeosciences* 9, 3185–3204 (2012).
11. Schimel D, Pavlick R, Fisher JB, Asner GP et al. Observing terrestrial ecosystems and the carbon cycle from space. *Glob.Change Biol* 21, 1762–1776 (2014).
12. Parazoo N, Commane R, Wofsy SC, Koven CD Detecting regional patterns of changing CO₂ flux in Alaska. *Proc. Natl. Acad. Sci* 113, 7733–7738 (2016). [PubMed: 27354511]
13. Grogan P. Cold season respiration across a Low Arctic landscape: The influence of vegetation type, snow depth, and interannual climatic variation. *Arctic, Antarct. Alp. Res* 44, 446–456 (2012).
14. Michaelson GJ, Ping CL Soil organic carbon and CO₂ respiration at subzero temperature in soils of Arctic Alaska. *J.G.R. Atmos* 108 (2005).
15. Rogers MC, Sullivan PF, Welker JM Evidence of nonlinearity in the response of net ecosystem CO₂ exchange to increasing levels of winter snow depth in the high Arctic of Northwestern Greenland. *Arct. Antarct. Alpine Res* 43, 95–106 (2011).
16. Wang T, Ciais P, Piao SL, Otle C, et al. Controls on winter ecosystem respiration in temperate and boreal ecosystems. *Biogeosciences* 8, 2009–2025 (2011).
17. Zona D, Gioli B, Commane R, Lindaas J, et al. Cold season emissions dominate the Arctic tundra methane budget. *Proc. Natl. Acad. Sci* 113, 40–45 (2016). [PubMed: 26699476]
18. Schaefer K and Jafarov E. A parameterization of respiration in frozen soils based on substrate availability. *Biogeosciences* 13, 1991–2001, doi:10.5194/bg-13-1991-2016 (2016).
19. Monson R, Lipson D, Burns SP, Turnipseed AA, et al. Winter forest soil respiration controlled by climate and microbial community composition. *Nature* 439, 711–714 (2006). [PubMed: 16467835]
20. Welker JM, Fahnestock JT, Jones MH Annual CO₂ flux in dry and moist arctic tundra: field responses to increases in summer temperatures and winter snow depth. *Clim. Chan* 44, 139–150 (2000).
21. Natali SM, Schuur EAG, Trucco C, Hicks Pries CE, et al. Effects of experimental warming of air, soil and permafrost on carbon balance in Alaskan tundra. *Glob. Chan. Biol* 17, 1394–1407 (2011).
22. Webb EE, et al. Increased wintertime CO₂ loss as a result of sustained tundra warming. *Biogeosciences* 12, 1–17 (2016).
23. Christiansen CT, Schmidt NM & Michelsen A. High Arctic dry heath CO₂ exchange during the early cold season. *Ecosystems* 15, 1083–1092 (2012).
24. Knutti R, Masson D & Gettelman A. Climate model genealogy: Generation CMIP5 and how we got there. *Geophys. Res. Lett* 40, 1194–1199 (2013).
25. Forkel M, et al. Enhanced seasonal CO₂ exchange caused by amplified plant productivity in northern ecosystems. *Science* 351, 696–699 (2016). [PubMed: 26797146]
26. Tucker C. Reduction of air- and liquid water-filled soil pore space with freezing explains high temperature sensitivity of soil respiration below 0 degrees C. *Soil Biol. Biochem* 78, 90–96 (2014).
27. Lorant MM, Abbott BW, Blok D, Douglas TA, et al. Reviews and Syntheses: Changing ecosystem influences on soil thermal regimes in northern high-latitude permafrost regions. *Biogeosciences* 15, 5287–5313. (2018).

28. Witze A. Snow-sensing fleet to unlock water's icy secrets. *Nature* 7, 1, doi: [10.1038/532017a](https://doi.org/10.1038/532017a) (2016).
29. Natali SM, Schuur EAG, Mauritz M, Schade JD, et al. Permafrost thaw and soil moisture driving CO₂ and CH₄ release from upland tundra. *J.G.R. Biogeosci* 120, 525–537 (2015).
30. Euskirchen ES, Bret-Harte MS, Shaver GR, Edgar CW, Romanovsky VE Long-term release of carbon dioxide from arctic tundra ecosystems in Alaska. *Ecosystems* 20, 960–974 (2017).
31. Tramontana G, et al. Predicting carbon dioxide and energy fluxes across global FLUXNET sites with regression algorithms. *Biogeosciences* 13, 4291–4313 (2016).
32. Koven CD, et al. Permafrost carbon-climate feedbacks accelerate global warming. *Proc. Natl. Acad. Sci* 108, 14769–14774 (2011). [PubMed: 21852573]
33. Slater AG, & Lawrence DM Diagnosing present and future permafrost from climate models. *J. Climate* 26, 5608–5623 (2013).
34. Vanhala P, Karhu K, Tuomi M, Bjorklof K, Fritze H, Liski J. Temperature sensitivity of soil organic matter decomposition in southern and northern areas of the boreal forest zone. *Soil Biol. Biochem* 40, 1758–1764 (2008).
35. Hugelius G. e. a. Estimated stocks of circumpolar permafrost carbon with quantified uncertainty ranges and identified data gaps. *Biogeosciences* 11, 6573–6593 (2014).
36. McGuire AD, et al. Dependence of the evolution of carbon dynamics in the northern permafrost region on the trajectory of climate change. *Proc. Natl. Acad. Sci*, doi:doi:[10.1073/pnas.1719903115](https://doi.org/10.1073/pnas.1719903115) (2018).
37. Qian H, Joseph R, Zeng N. Enhanced terrestrial carbon uptake in the Northern High Latitudes in the 21st century from the Coupled Carbon Climate Model Intercomparison Project model projections. *Glob. Chan. Biol* 16, 641–656, doi:[10.1111/j.1365-2486.2009.01989.x](https://doi.org/10.1111/j.1365-2486.2009.01989.x).
38. Starr GO, et al. Photosynthesis of Arctic evergreens under snow: Implications for tundra ecosystem carbon balance. *Ecology* 84, 1415–1420 (2003).
39. Treat CC, Bloom AA & Marushchak ME Nongrowing season methane emissions—a significant component of annual emissions across northern ecosystems. *Glob. Chang. Biol* 24, 3331–3343 (2018). [PubMed: 29569301]
40. Walter Anthony K, et al. 21st-century modeled permafrost carbon emissions accelerated by abrupt thaw beneath lakes. *Nat. Commun* 9 (2018).

Methods References

41. Brown J, Ferrians O, Heginbottom J & Melnikov E. Circum-Arctic map of permafrost and ground-ice conditions, version 2 (2002).
42. Brodzik MJ, Billingsley B, Haran T, Raup B & Savoie MH EASE-Grid 2.0: Incremental but significant improvements for Earth-gridded data sets. *ISPRS Int. J. Geo-Information* 1, 32–45 (2012).
43. R Core Team R: A language and environment for statistical computing. (2016).
44. Ridgeway G. Generalized Boosted Models: A guide to the gbm package. 1–12 (2007).
45. Elith J, Leathwick JR & Hastie T. A working guide to boosted regression trees. *J. Anim. Ecol*, 802–813 (2008). [PubMed: 18397250]
46. Hijmans RJ, Phillips S, Leathwick J & Elith J. R “dismo” package. (2017).
47. Bronaugh DWR “zyp” trends package. (2017).
48. Rogers BM, et al. Impacts of climate change on fire regimes and carbon stocks of the U.S. Pacific Northwest. *J. Geophys. Res. Biogeosciences* 116 (2011).
49. Leathwick JR, Elith J, Francis MP, Hastie T & Taylor P. Variation in demersal fish species richness in the oceans surrounding New Zealand: An analysis using boosted regression trees. *Mar. Ecol. Prog. Ser* 321, 267–281 (2006).

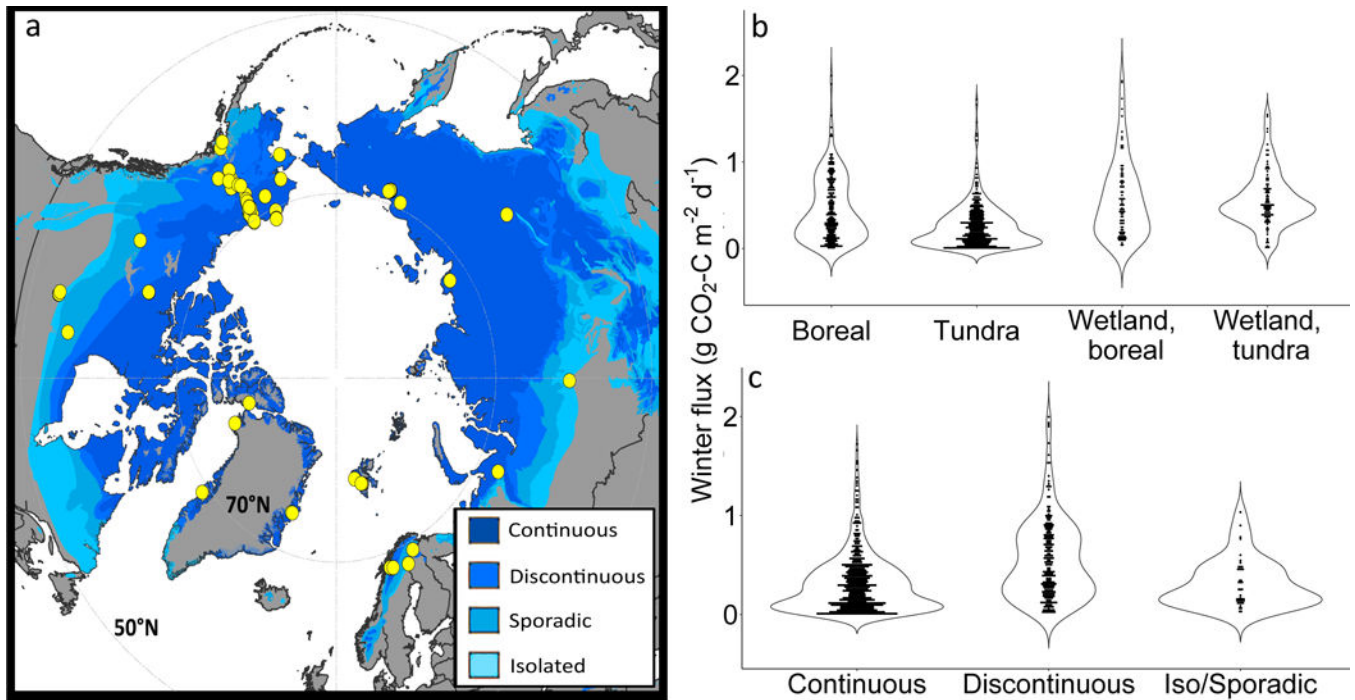


Fig. 1. Distribution of *in situ* data included in this winter CO₂ flux synthesis.

(a) Locations of *in situ* winter CO₂ flux data (yellow circles) in this synthesis include (b) upland and wetland sites in boreal and tundra biomes located (c) within the northern permafrost region⁴¹. Violin plots (b,c) depict magnitude and distribution density (width; dots are monthly aggregated data) of *in situ* data used in our machine-learning model.

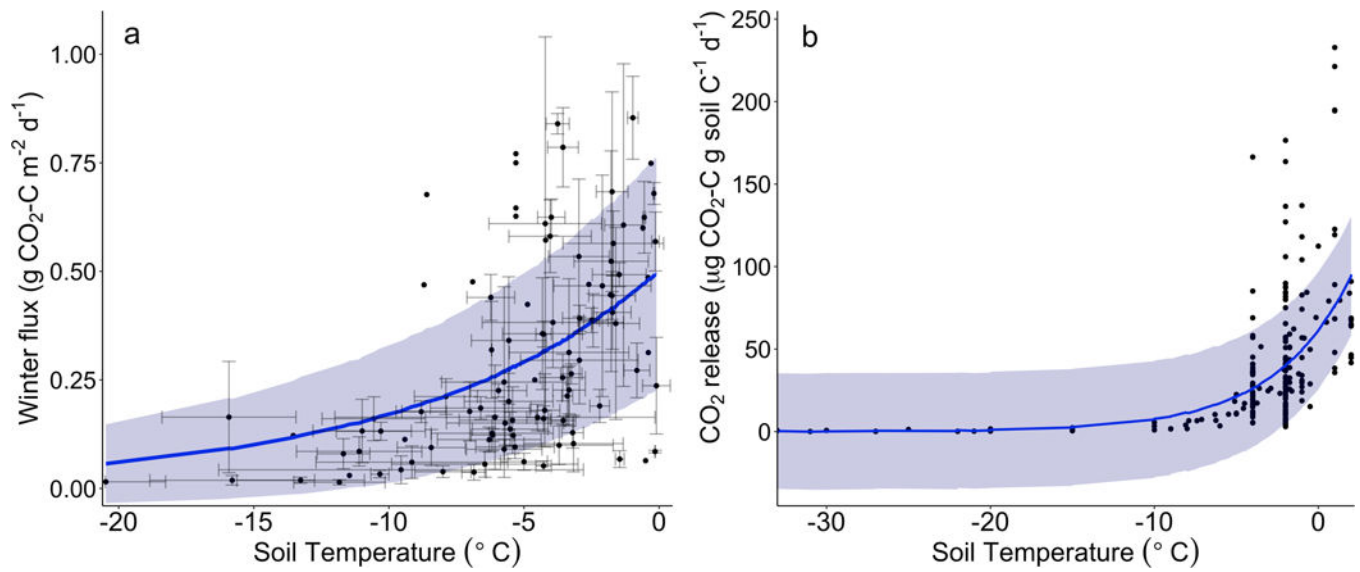


Fig. 2. Effect of soil temperature on CO₂ release from soils.

(a) Relationships between *in situ* soil temperature (~ 10 cm average depth) and CO₂ fluxes and (b) temperature and CO₂ released from lab incubations. Shading represents the standard deviation of an exponential model, which, for *in situ* fluxes, was fit to mean CO₂ flux from each sample location (symbols shown with standard error). Note that the different soil temperature scales between panels reflect data ranges.

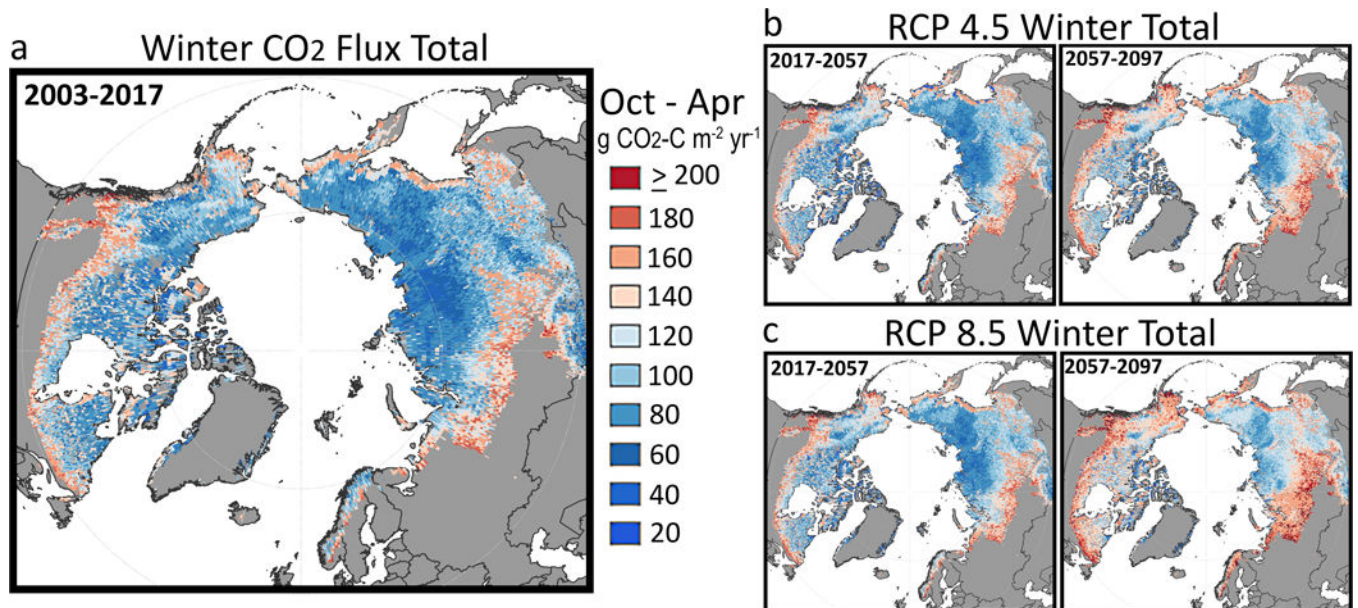


Fig. 3. Pan-Arctic winter CO₂ emissions under current and future climate scenarios.

(a) Average annual winter (October - April) CO₂ emissions estimated for the permafrost region for the baseline years 2003–2017. Cumulative winter CO₂ fluxes under (b) RCP 4.5 and (c) RCP 8.5 scenarios over an 80-year period (2017–2057 and 2057–2097). Fluxes are reported on an annual basis (g CO₂-C m⁻² yr⁻¹).

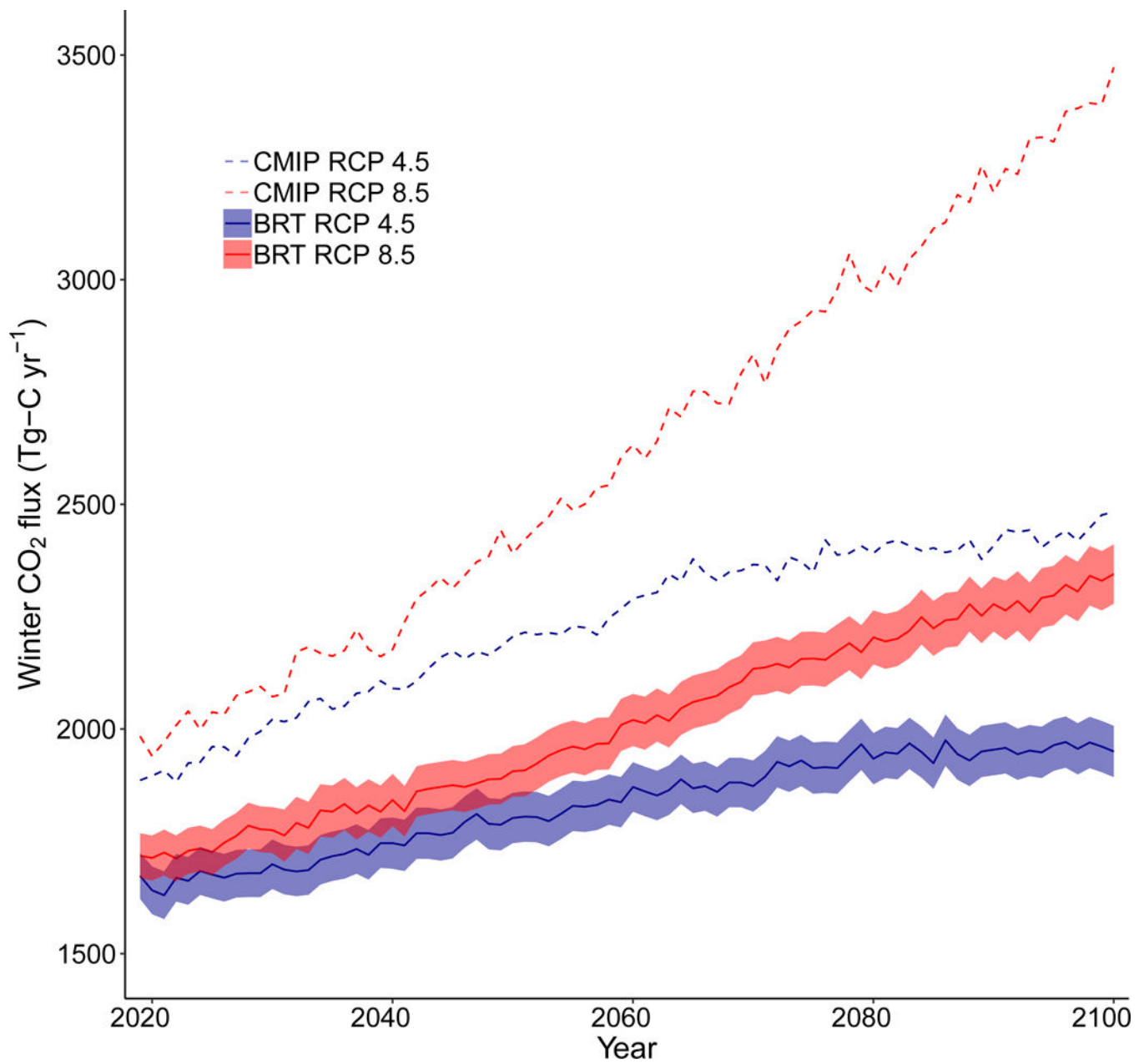


Fig. 4. Projected annual CO₂ emissions during the winter for the northern permafrost region. Solid lines represent BRT modeled results through 2100 under RCP 4.5 (blue solid line) and RCP 8.5 (red solid line), with bootstrapped 95% confidence intervals indicated by shading. For reference, CMIP5 ensemble respiration for RCP 4.5 and 8.5 are also shown (dashed lines).